

# THE INTERNAL STRUCTURE AND FORMATION OF EARLY-TYPE GALAXIES: THE GRAVITATIONAL-LENS SYSTEM MG2016+112 AT $Z=1.004$

TOMMASO TREU

California Institute of Technology, Astronomy, mailcode 105–24, Pasadena, CA 91125

LÉON V.E. KOOPMANS

California Institute of Technology, Theoretical Astrophysics Including Relativity (TAPIR), mailcode 130–33,

Pasadena, CA 91125

*submitted to ApJ*

## ABSTRACT

We combine our recent measurements of the velocity dispersion and the surface brightness profile of the lens galaxy D in the system MG2016+112 ( $z = 1.004$ ) with constraints from gravitational lensing to study its internal mass distribution. We find that: *i*) dark matter accounts for  $>50\%$  of the total mass within the Einstein radius (99% CL), whereas  $\sim 75\%$  is the more likely contribution. In particular, we can exclude at the  $8\text{-}\sigma$  level that mass follows light inside the Einstein radius with a constant mass-to-light ratio (M/L). *ii*) the total mass distribution inside the Einstein radius is well-described by a density profile  $\propto r^{-\gamma'}$  with an effective slope  $\gamma' = 2.0 \pm 0.1 \pm 0.1$ , including random and systematic uncertainties. *iii*) The offset of galaxy D from the local Fundamental Plane independently constrains the stellar M/L, and matches the range derived from our models, leading to a more stringent lower limit of  $>60\%$  (99% CL) on the fraction of dark matter within the Einstein radius.

Under the assumption of adiabatic contraction, we show that the inner slope of the dark matter halo before the baryons collapsed to form the lens galaxy is  $\gamma_i < 1.4$  (68% CL), only marginally consistent with the highest-resolution cold dark matter simulations that indicate  $\gamma_i \sim 1.5$ . This might indicate that either adiabatic contraction is a poor description of early-type galaxy formation or that additional processes play a role as well. Indeed, the apparently isothermal density distribution inside the Einstein radius, is not a natural outcome of adiabatic contraction models, where it appears to be a mere coincidence. By contrast, we argue that isothermality might be the result of a stronger coupling between luminous and dark-matter, possibly the result of (incomplete) violent relaxation processes during the formation of the innermost regions of the galaxy. We briefly discuss the importance of our results for lens statistics and the determination of the Hubble Constant from gravitational-lens time delays.

*Subject headings:* gravitational lensing — galaxies: elliptical and lenticular, cD — galaxies: evolution — galaxies: formation — galaxies: structure

## 1. INTRODUCTION

Understanding the internal structure of galaxies, is crucial to explain the variety of their observed morphologies and the physical processes that created them. It also provides an opportunity to test physics on galactic scales.

Because early-type (E/S0) galaxies are relatively simple systems, dynamical modeling of their internal structure can be attempted with hope for success (e.g. de Zeeuw & Franx 1991; Bertin & Stiavelli 1993; Merritt 1999). Knowledge of this internal structure provides a vital discriminant to the processes involved in their formation (e.g. van Albada 1982), which is currently a highly controversial issue (e.g. Schade et al. 1999).

In particular, in the cold dark matter (CDM) cosmological model, galaxies are embedded in dark matter halos, which dominate the total mass of the system and have a characteristic mass distribution (Navarro, Frenk & White 1997, hereafter NFW; Moore et al. 1998; Bullock et al. 2001; Ghigna et al. 2000). Measuring the distribution of dark matter in E/S0 galaxies would therefore not only shed light on their formation history, but also provide a powerful test of the CDM cosmological model. This test is

similar, but complementary in the scales and physical conditions probed, to the still controversial tests performed using the kinematics of low surface-brightness and dwarf galaxies (e.g. McGaugh & de Blok 1998; van den Bosch et al. 2000; Swaters, Madore & Trewhella 2000; Salucci & Burkert 2000; Borriello & Salucci 2001; van den Bosch & Swaters 2001; de Blok et al. 2001; de Blok & Bosma 2002; Jimenez, Verde & Peng 2002).

Unfortunately, E/S0 galaxies generally lack simple dynamical tracers at large radii, such as HI in spiral galaxies, and little is known about their kinematics beyond the region dominated by stellar mass (1–2 effective radii,  $R_e$ ). Hence, the amount and distribution of dark matter within E/S0 galaxies remain to date poorly constrained even in the local Universe (e. g. Bertin et al. 1994; Franx et al. 1994; Carollo et al. 1995; Rix et al. 1997; Gerhard et al. 2001). In a few exceptional cases kinematic tracers at large radii have been found and used to investigate the presence and distribution of dark matter halos (e. g. Mould et al. 1990; Franx, van Gorkom & de Zeeuw 1994; Hui et al. 1995; Arnaboldi et al. 1996). However, these methods do not seem likely to be applicable at significant look-back

<sup>1</sup> Based on observations collected at W. M. Keck Observatory, which is operated jointly by the California Institute of Technology and the University of California, and with the NASA/ESA Hubble Space Telescope, obtained at STScI, which is operated by AURA, under NASA contract NAS5-26555.

times and thus to investigate the evolution of the internal structure of E/S0.

An independent measure of the mass distribution of E/S0 galaxies is provided by gravitational lensing, which is not sensitive to its dynamical state. For example, gravitational lensing alone has been used to show the existence of dark matter in individual E/S0 galaxies (e. g. Kochanek 1995) and recently to constrain the dark matter halo profile from gravitational-lens statistics (Keeton 2001). The combination of dynamical and lensing analyses can significantly reduce the degeneracies inherent to each method and result in tighter constraints on the dark-matter distribution, as well as on the luminous and total mass distribution. In addition, most lenses are found at intermediate redshift ( $0.1 < z < 1$ ) and therefore offer the possibility to probe the mass distribution at significant look-back times.

### 1.1. *The Lenses Structure and Dynamics (LSD) Survey*

To investigate the internal structure of E/S0 galaxies and test CDM predictions, we have started a program to measure the kinematic profiles of a sample of E/S0 galaxies that are also gravitational lenses; the *Lenses Structure and Dynamics Survey* (hereafter the LSD Survey<sup>2</sup>). By means of deep spectroscopy using the Echelette Imager Spectrograph (ESI) at the W. M. Keck II Telescope, we are deriving extended kinematic profiles (beyond the effective radius) for the nearest and brightest lenses, along major and sometimes minor axes, while for the most distant and faint ones we are measuring a luminosity-weighted velocity dispersion. The ultimate aim of the LSD Survey is to produce a database of measurements of internal kinematics for the largest possible number of E/S0 lens galaxies, covering a range of redshifts and masses.

The target lenses have to: *i*) have E/S0 morphology, as determined from Hubble Space Telescope (HST) images; *ii*) be relatively undisturbed by the light of the lensed object at ground based resolution; *iii*) be relatively isolated, since a nearby cluster, large group, or massive companion, would introduce additional uncertainties in the measurement of the mass of the lens; *iv*) be bright enough that accurate internal kinematics can be determined in a few hours of integration. A preference is given to objects where the redshift of the background source is known. If the redshift of the source is not known and the source is bright enough that the redshift can be determined in a few hours of integration time, the redshift is also determined.

In addition to help clarifying the origin of E/S0 galaxies, other important results will be obtained if a better understanding of the internal structure of E/S0 and its evolution with redshift is achieved. For example we can mention the determination of the Hubble constant from time-delay, and the calculations of lens cross-sections.

### 1.2. *A case study: MG2016+112*

In a previous paper (Koopmans & Treu 2002; hereafter KT02) we described the Keck and HST observations of the E/S0 lens galaxy D in MG2016+112, the most distant spectroscopically confirmed lens galaxy known ( $z = 1.004$ ). A review of the current observations of this system can be found in Koopmans et al. (2002; hereafter K02), who also propose a detailed lens model, where the image

separation is caused predominantly by galaxy D, and predict a central velocity dispersion  $\sigma = 320\text{--}340 \text{ km s}^{-1}$  for an isothermal total mass distribution. This value should correspond closely to the central stellar velocity dispersion (e. g. Kochanek 1994; Kochanek et al. 2000). Our direct measurement shows that D is indeed a massive old E/S0 galaxy, possibly embedded in a proto-cluster.

In this paper we present an analysis of the internal structure of galaxy D, based on the observed velocity dispersion and the exquisite HST images available from the CASTLES database. In particular, we focus on the shape of the dark matter halo and the density profile of the total mass distribution. Apart for its high redshift (corresponding to  $\sim 8$  Gyr look-back time), this system is particularly interesting because its Einstein radius ( $R_{\text{Einst}} = 13.7 \text{ kpc}$ ) is much larger than the effective radius of the lens galaxy ( $R_e = 2.7 \text{ kpc}$ ). For this reason, we can use gravitational lensing to probe the mass distribution to much larger radii that is typically done even in local E/S0.

The paper is organized as follows. The modeling is described in Sec. 2, the dark and luminous matter distributions derived in Sec. 3 and compared to CDM predictions in Sec. 4. Sec. 5 uses the results found for MG2016+112 to predict observables for other systems. Discussion and conclusions are given in Sec. 6. Throughout the paper  $r$  is the radial coordinate in 3-D space, while  $R$  is the radial coordinate in 2-D projected space. For definiteness, we assume the Hubble Constant, the matter density, and the cosmological constant to be  $H_0 = 65 \text{ km s}^{-1} \text{ Mpc}^{-1}$ ,  $\Omega_m = 0.3$  and  $\Omega_\Lambda = 0.7$ , respectively.

## 2. MODELS

Based on the lens models in K02, one finds a total mass enclosed within the Einstein radius,  $M(< R_{\text{Einst}}) \equiv M_E = 1.1 \times 10^{12} M_\odot$ . The enclosed mass has been corrected for the slight ellipticity of the lens potential and, because the source lies almost on the observer-lens axis, is nearly independent of the mass distribution assumed for the lens model (e.g. Schneider, Ehlers & Falco 1992; Chapter 8). An error of  $\sim 10\%$  is assumed for the enclosed mass (K02). Later, we will estimate the effect of this potential systematic error on our conclusions and show it to be negligible.

The total luminosity of the system is  $(1.6 \pm 0.2) 10^{11} L_{\odot, B}$  (KT02), implying an average mass-to-light ratio  $M/L_B = 8 \pm 1 M_\odot/L_{\odot, B}$  inside the Einstein radius. This value is similar to the values found for the stellar populations of local E/S0 galaxies (e.g. Gerhard et al. 2001). However, considering the much smaller age of the stellar populations of galaxy D – estimated to be  $3 \pm 0.8$  Gyr and not larger than the age of the Universe at  $z = 1.004$  ( $\sim 6$  Gyr; KT02) – the stellar M/L ratio of galaxy D must be smaller than in the local Universe, due to luminosity evolution of the stellar population. Given the large value of M/L, we conclude that a significant amount of dark matter is likely to be present inside  $R_{\text{Einst}}$  and we choose to describe the mass distribution of MG2016+112 with two spherical components, one for the luminous matter and one for the dark matter halo. In particular, we model the luminous mass distribution with a Hernquist (1990) model

$$\rho_L(r) = \frac{M_* r_*}{2\pi r(r + r_*)^3}, \quad (1)$$

<sup>2</sup> see ‘www.astro.caltech.edu/~tt/LSD’ or ‘www.its.caltech.edu/~koopmans/LSD’

that well reproduces the  $R^{1/4}$  surface brightness profile for  $r_* = R_e/1.8153$  ( $M_*$  is the total stellar mass) and is simple to treat analytically (e.g. Ciotti, Lanzoni & Renzini 1996). The dark matter halo is modeled as

$$\rho_d(r) = \frac{\rho_{d,0}}{(r/r_b)^\gamma (1 + (r/r_b)^2)^{\frac{3-\gamma}{2}}} \quad (2)$$

which closely describes a NFW profile for  $\gamma = 1$ , and has the typical asymptotic behavior at large radii found from numerical simulations of dark matter halos  $\propto r^{-3}$  (e. g. Ghigna et al. 2000). Note that, for  $r_b$  significantly exceeding  $R_{\text{Einst}}$ , the particular choice of the outer slope has only a negligible effect on  $M_E$  or the kinematics of the lens galaxy. In particular, for  $r_b \rightarrow \infty$  and  $\gamma = 2$  Eq. 2 reduces to a singular isothermal sphere, a functional form often used to describe dark matter halos. In addition, Eq. 2 provides a simple parametrization of the controversial inner slope for  $r < r_b$ , the region better constrained by our observations. The length scale ( $r_b$ ) and the density scale ( $\rho_{d,0}$ ) determine the virial mass of the dark matter halo (e. g. Bullock et al. 2001).

The velocity dispersion is computed solving the spherical Jeans equation (e.g. Binney & Tremaine 1987), assuming an Osipkov-Merritt (Osipkov 1979; Merritt 1985a,b) parametrization of the anisotropy  $\beta$ :

$$\beta(r) = 1 - \frac{\sigma_\theta^2}{\sigma_r^2} = \frac{r^2}{r^2 + r_i^2}, \quad (3)$$

where  $\sigma_\theta$  and  $\sigma_r$  are the tangential and radial component of the velocity dispersion. Finally, the velocity dispersion as observed through our spectroscopic aperture ( $\equiv \sigma_{ap}$ ; effectively corresponding to a circular aperture of radius  $0''.65 \sim 2R_e$ ) is computed as the average of the projected velocity dispersion weighted by the surface brightness.

### 3. LUMINOUS AND DARK MATTER IN MG2016+112

#### 3.1. Constraints from kinematics, lensing geometry, and surface brightness distribution

The effective radius and the total mass within  $R_{\text{Einst}}$  ( $M_E$ ) are fixed by the observations (KT02). This leaves four free parameters in the model: the inner slope ( $\gamma$ ) of the dark matter halo, the length scale of the dark matter component ( $r_b$ ), the mass-to-light ratio of the luminous component ( $M_*/L_B$ ) and the anisotropy radius ( $r_i$ ). In Fig. 1 we show the likelihood contours<sup>3</sup> of  $\gamma$  and  $M_*/L_B$ , given the observed velocity dispersion ( $\sigma_{ap} = 304 \pm 27 \text{ km s}^{-1}$ ) for a range of values of  $r_b$ . Since changing  $r_i$  has very little effect on the likelihood contours, only the ones obtained for  $r_i = R_e$  are shown (see further discussion in the rest of this section and in Sec. 5).

Two main conclusions can be drawn from Fig. 1. First, since  $M_*/L_B \lesssim 4 M_\odot/L_{\odot,B}$  (99% CL), i.e. smaller than the total  $M/L_B = 8 \pm 1 M_\odot/L_{\odot,B}$ , dark matter is present within  $R_{\text{Einst}}$  and contributes  $\gtrsim 50\%$  (99% CL) of the mass. As an independent check, if we assume that  $M_E$  arises from the luminous component only with a constant  $M_*/L_B = 8 M_\odot/L_{\odot,B}$ , we find  $\sigma_{ap} = 530 \text{ km s}^{-1}$  (virtually independent of the isotropy radius), inconsistent with the

observed value at better than  $8\sigma$ . Second, we find that when  $M_*/L_B \rightarrow 0$  and  $r_b \rightarrow \infty$ ,  $\gamma = 2.0 \pm 0.1$  ( $1-\sigma$  error). In other words, the total mass can be very well described by a single power-law density distribution  $\rho_t \propto r^{-\gamma'}$  with effective<sup>4</sup> slope  $\gamma' = 2.0 \pm 0.1$ . A systematic error of 10% on  $M_E$  changes the inferred slope by only 0.05, whereas a 20% error ( $1-\sigma$ ) on  $R_e$  affects the result by only 0.02. Similarly, a 20% error ( $1-\sigma$ ) on the assumed aperture radius of  $0''.65$  changes the result by 0.03. Even a factor 10 deviation from  $r_i = R_e$  results in  $\lesssim 0.05$  error, although the effect on the central velocity dispersion<sup>5</sup>  $\sigma$  in that case is much more profound, with significantly larger values of  $\sigma$  for smaller  $r_i$  (i.e. more radial orbits, see Fig. 4). Hence,  $\gamma'$  is robust against reasonable changes in the parameters  $r_i$ ,  $R_e$ ,  $M_E$ , the aperture radius, and  $r_b \gtrsim R_{\text{Einst}}$ .

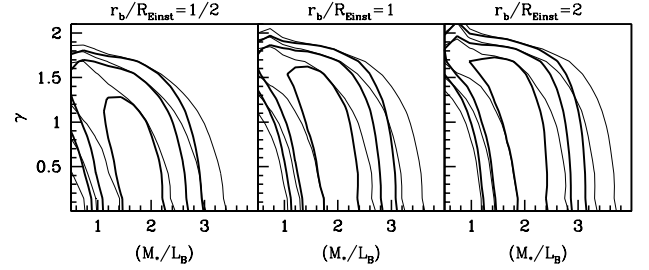


FIG. 1.— Constraints on the inner slope of the dark matter halo ( $\gamma$ ) and the stellar mass-to-light ratio ( $M_*/L_B$ , in solar units). Thin contours represent the 68%, 95%, 99% confidence limits given  $M_E$ ,  $R_e$  and  $\sigma_{ap}$ . The thick contours represent the same limits, if the independent measurement of  $M_*/L_B$  from the evolution of the FP is included (Eq. 6). The subpanels present the results for different values of the dark-matter length scale ( $r_b$ ). The contours change negligibly for different values of the anisotropy radius  $r_i$  ( $r_i/R_e = 0.5, 1, 2$ ), thus only the case  $r_i/R_e = 1$  is shown. See Sec. 3 for a detailed discussion.

We can make a very simple argument to understand why the effective slope is so tightly constrained by our observations. For a total mass profile  $\rho_{\gamma'} \propto r^{-\gamma'}$  the enclosed mass is  $M(< r) \propto r^{3-\gamma'}$ . Therefore, the mass within the effective radius ( $M_e$ ) depends on the mass within the Einstein radius ( $M_E$ ) as

$$M_e = M_E \left( \frac{R_e}{R_{\text{Einst}}} \right)^{3-\gamma'} \equiv x_E^{\gamma'-3}, \quad (4)$$

where  $x_E \equiv R_{\text{Einst}}/R_e$  has been introduced for simplicity of notation. Hence, assuming  $M_e \propto \sigma^2$  for a given  $R_e$ ,

$$\delta\gamma' = 2 \log(1 + \frac{\delta\sigma}{\sigma}) \log(x_E)^{-1} \approx \frac{2\delta\sigma}{\sigma \log(x_E)}, \quad (5)$$

where  $\delta\gamma'$  and  $\delta\sigma$  are the errors on the effective slope and velocity dispersion, respectively. Using the values for MG2016+112 in Eq. 5 we recover  $\delta\gamma' \approx 0.1$  in good agreement with the error inferred from our model.

#### 3.2. Further constraints: the evolution of the Fundamental Plane

Recent studies have shown that E/S0 galaxies both in clusters and in the field define a tight Fundamental Plane

<sup>3</sup> Gaussian error distributions are assumed.

<sup>4</sup> We use the term effective slope to emphasize that this is the slope that we get with a single power law. The real mass distribution could change slope between the constraints given within the spectroscopic aperture radius and at  $R_{\text{Einst}}$ , as long as the effective trend is preserved.

<sup>5</sup> defined as the luminosity-weighted velocity dispersion within a circular aperture of radius  $R_e/8$

(FP; Dressler et al. 1987; Djorgovski & Davis 1987) out to  $z \sim 0.7 - 0.8$  (van Dokkum et al. 1998; Treu et al. 1999, 2002), with slopes very similar to the ones observed in the local Universe. Assuming that galaxy D in MG2016+112 lies on a FP with slopes as in the local Universe, we can obtain an additional constraint on its internal structure. In fact, the evolution of the intercept of the FP with redshift can be related to the evolution of the average effective mass to light ratio ( $\Delta \log M/L_B$ ; see e. g. Treu et al. 2001 for discussion). For D we obtained  $\Delta \log M/L_B = -0.62 \pm 0.08$ , i.e. somewhat intermediate between the cluster and field value (KT02). We can use this measurement to infer  $M_*/L_B$  of D assuming that

$$\log(M_*/L_B)_z = \log(M_*/L_B)_0 + \Delta \log(M/L_B), \quad (6)$$

where the second term on the right hand side of the equation is measured from the evolution of the FP. The first term on the right hand side of the equation can be measured for local E/S0 galaxies: for example using the data from Gerhard et al. (2001; and references therein), we find a good correlation between  $\sigma^2 R_e$  and  $M_*/L_B$ . Using the values of MG2016+112, this correlation yields  $M_*/L_B(z=0) = 7.3 \pm 2.1 M_\odot/L_{\odot,B}$ , where the error includes the contribution from the scatter between dynamical and stellar population measurements<sup>6</sup>. Hence, from Eq. 6 we find  $M_*/L_B(z=1.004) = 1.8 \pm 0.7 M_\odot/L_{\odot,B}$ . We note two things: (i) the value  $M_*/L_B = 8 M_\odot/L_{\odot,B}$  required to explain the enclosed mass solely by luminous matter is inconsistent with the above, independently-derived, value at the  $9-\sigma$  level, and (ii) the allowed range of  $M_*/L_B$  found from our dynamical modeling (Fig. 1) overlaps very nicely with the value derived from the evolution of the FP. Using this additional constraint we obtain the probability contours plotted as solid lines in Fig. 1. Again, the results depend very modestly on the anisotropy radius, while the slope  $\gamma$  becomes steeper as  $r_b$  increases. In general,  $\gamma = 2$  can be ruled out at better than  $2-4 \sigma$  (depending on  $r_b$ ), and therefore the dark matter profile is *not* isothermal.

Let us now examine the total mass distribution of the two-component model in more detail with the help of the quantities plotted in Fig. 2. First (lower panel), we show the density profiles of a characteristic best-fitting model ( $r_b = 2R_e$ ,  $r_i = R_e$ ;  $M_*/L = 1.8 M_\odot/L_{\odot,B}$ ). Even though luminous and dark matter themselves are not isothermally distributed, the total mass distribution is very close to isothermal, confirming what we found in Section 3.1. Second (middle panel), we show the relative difference between a power law mass profile  $\rho_{\gamma'} \propto r^{-\gamma'}$  and the total mass profile obtained with our two-component model. A profile with  $\gamma' = 2$  describes the total mass profile very well. By contrast,  $\gamma' = 1.8$  or  $\gamma' = 2.2$  result in significantly worst representations of the total mass profile. Third (upper panel), we compare the luminosity-weighted velocity dispersion profile of our two-component model with those obtained for  $\gamma' = 1.8, 2.0$  and  $2.2$ . The  $\gamma' = 2$  power law mass profile and the two-component model produce almost identical velocity dispersion profiles, while  $\gamma' = 1.8, 2.2$  are clearly inconsistent with the observed  $\sigma_{ap}$  (point with error bar in the plot). For completeness, we note that we find  $\sigma/\sigma_{ap} = 1.06$ , consistent with our assumption of  $1.08 \pm 0.05$  in KT02.

Finally, we check that our best-fitting models corre-

spond indeed to physical solutions in the sense that they can be generated by a positive distribution function (i.e. they are *consistent* models, see e.g. Ciotti 1999 and references therein for discussion). For our choice of values of  $r_i/R_e$ , a luminous Hernquist model embedded in a total isothermal mass distribution always satisfies the sufficient condition given in Eq. 6 of Ciotti (1999), and therefore our best-fitting models are *consistent*.

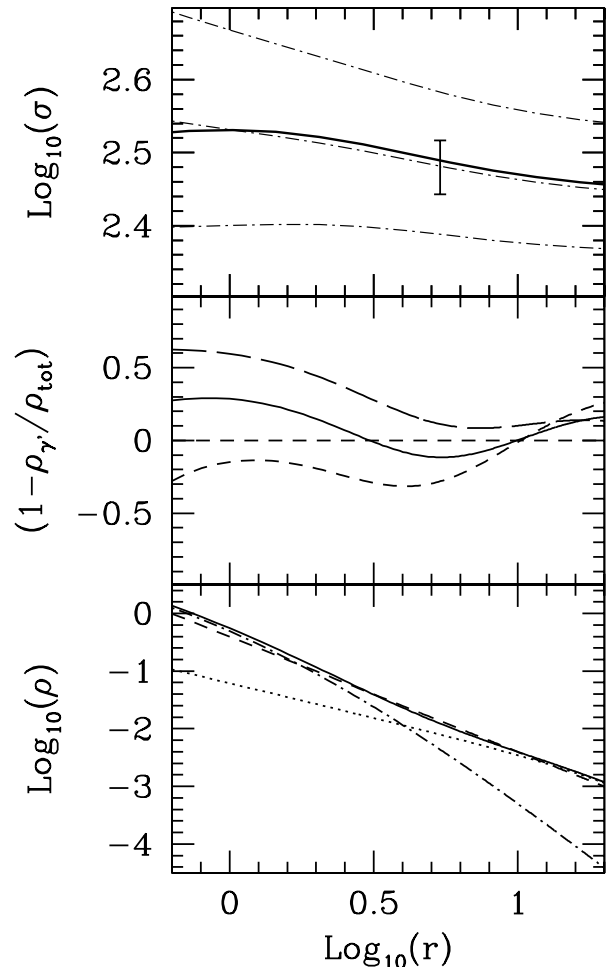


FIG. 2.— Dark and luminous matter best-fit density (in units of  $10^{10} M_\odot \text{ kpc}^{-3}$ ) and velocity dispersion profiles (in  $\text{km s}^{-1}$ ) as function of radius (in kpc). Lower panel: Density profile of the luminous component (dot-dashed), of the dark matter halo (dotted) and the sum of the two (solid) for several characteristic best-fitting models. An  $r^{-2}$  density profile (dashed) reproduces the total density profile remarkably accurately. Middle panel: Relative residuals of the total mass distribution ( $\rho_{tot}$ ) with respect to power laws  $\rho_{\gamma'} = r^{-\gamma'}$ , with  $\gamma' = 2.2, 2, 1.8$  from top to bottom. Upper panel: Luminosity-weighted velocity dispersion profile as a function of circular aperture. The solid lines are obtained for the best-fitting two-component model. The thin dot-dashed lines correspond to power-law mass distributions with  $\gamma' = 2.2, 2, 1.8$  from top to bottom. The error bar represents our measurement  $\sigma_{ap} = 304 \pm 27 \text{ km s}^{-1}$ . We assume  $M_*/L_B = 1.8 M_\odot/L_{\odot,B}$ .

#### 4. COMPARISON WITH CDM MODELS

In order to make a proper comparison with CDM predictions, we have to consider that the universal profiles

<sup>6</sup> A very similar result is obtained by taking simply the average stellar M/L of the sample  $7.8 \pm 2.7 M_\odot/L_{\odot,B}$ .

of dark matter halos can be significantly modified by the formation of a galaxy within the halo. A simple treatment of this phenomenon can be given by assuming the so-called “adiabatic approximation” (Blumenthal et al. 1986; see also Mo, Mao & White 1998). Under this approximation, for any given initial mass distribution (baryons are assumed to follow dark matter at the beginning) we can calculate the final dark matter distribution after the galaxy has collapsed, for example to an Hernquist mass distribution (e. g. Keeton 2001; see also Rix et al. 1997). Here, we use the approximation backwards to recover the initial dark matter density profile. In order to facilitate comparison to CDM predictions, we fit the same functional form as in Eq. 2 to the initial density profile by minimizing the fractional difference in density integrated over 0–100 kpc, and derive the initial length scale  $r_{b,i}$  and an initial slope  $\gamma_i$ . Although it was not guaranteed *a priori*, we find that this form gives a reasonable description of the initial density profile as well.

Before proceeding to the calculation, we reduce the degrees of freedom of the problem by noticing that CDM models indicate that the length scale of systems as massive as galaxy D should be significantly larger than  $\sim 15$  kpc, even at  $z \sim 1$  (Bullock et al. 2001). Therefore, in the spirit of the comparison with CDM predictions, we can limit our parameter space to  $r_b > R_{\text{Einst}}$ , where the results depend very little on the exact value of  $r_b$ . The length scale does not change significantly ( $< 30\%$  depending on the slope for  $r_{bi} < 40$  kpc) during collapse, therefore our assumption on  $r_b$  being large because  $r_{b,i}$  is large is justified in this context. For definiteness, we pick  $r_b = 2R_{\text{Einst}}$  so that the observed profiles are shown in Fig. 1 and 2. With this assumption, the initial slope  $\gamma_i$  depends only on the observed slope  $\gamma$  and on  $M_*/L_B$ .

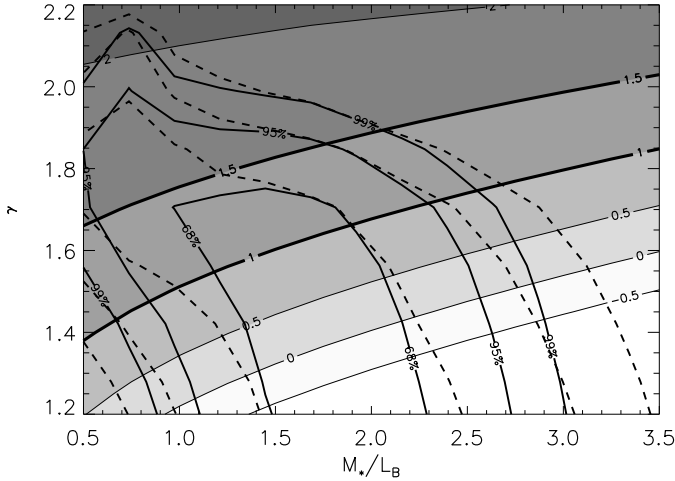


FIG. 3.— Relation between the final ( $\gamma$ ) and the initial ( $\gamma_i$ ) inner slope of the CDM dark-matter halo of galaxy D in MG2016+112, and the stellar mass-to-light ratio ( $M_*/L_B$ ), based on a simple adiabatic contraction model (see text). The loci corresponding to different initial slopes are shown, labeled by  $\gamma_i$ . In particular, the two thick contours labeled 1.0 and 1.5 ( $=\gamma_i$ ) indicate the NFW and Moore et al. (1998) profiles, respectively. The probability contours given the observations of MG2016+112 for a model with  $r_d = 2R_{\text{Einst}}$  and  $r_i = R_e$  (see Fig. 1) are overplotted and labeled by the probability level. As in Fig. 1 solid lines include the constraint from the FP evolution, dashed lines do not.

In Fig 3 we show the contour levels of  $\gamma_i$  in the  $\gamma - M_*/L_B$  plane. As  $M_*/L_B \rightarrow 0$ , the effect of baryons

becomes negligible and  $\gamma \rightarrow \gamma_i$ . On the other hand, as  $M_*/L_B$  increases, the collapse becomes increasingly important and flatter initial dark matter halo correspond to increasingly steeper final halos. To constrain  $\gamma_i$  with the observations, we overlay the likelihood contours of  $\gamma - M_*/L_B$  derived from our dynamical model (Fig. 1), and consider only the portion of the  $\gamma_i$  contours enclosed by the likelihood contours. Considering only monotonically decreasing profiles, the range  $\gamma_i = 0.0 - 1.4$  maps onto a very tight range of final slopes  $\gamma \approx 1.30 - 1.75$ . In conclusion – within the context of this simple adiabatic contraction model –  $\gamma_i = 1.5$  is only marginally consistent with our observations, whereas  $\gamma_i = 1$  fits within the 68% likelihood contour.

#### 5. KINEMATICS OF HERNQUIST LUMINOSITY DENSITY PROFILES IN A LOGARITHMIC GRAVITATIONAL POTENTIAL

In Sec. 3 we have shown that the total mass distribution of galaxy D is well described by an isothermal sphere in the range  $\sim 1$ –15 kpc. Here, we generalize the results found for galaxy D to compute the velocity dispersion profiles that we expect to find for other lens E/S0 galaxies.

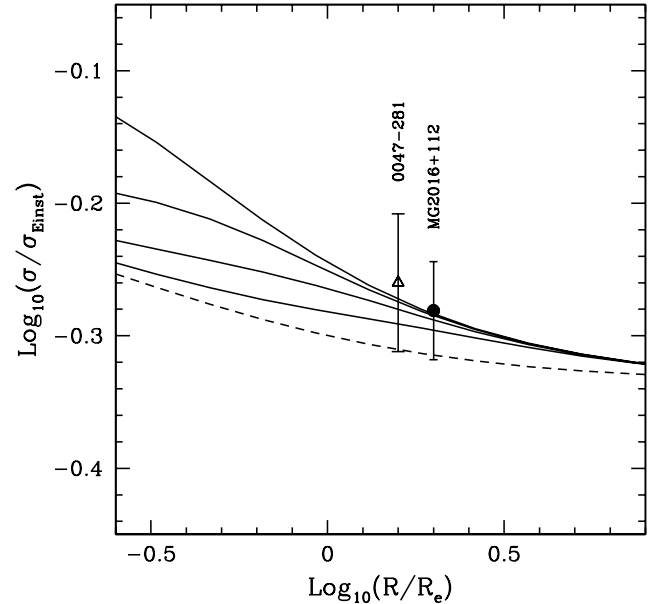


FIG. 4.— Luminosity-weighted velocity dispersion profile for a Hernquist luminosity-density profile in logarithmic potential. The axes are scaled in units of  $R_e$  and  $\sigma_{\text{Einst}}$  (see text). From top to bottom curves are shown for  $r_i/R_e = 0.2, 0.5, 1, 2, \infty$  (where  $\infty$  corresponds to isotropic models). Note the smaller effect of changing anisotropy radius  $r_i$ , as compared to changing the effective slope  $\gamma'$  of the total mass distribution (upper panels in Fig. 2; to facilitate comparison the two figures show the same range of velocity dispersion and radius). Our measurement of MG2016+112 is shown as a filled circle. The value for 0047-281 using data from Warren et al. (1998) and Kochanek et al. (2000) is shown as an open triangle.

Let us assume that E/S0 galaxies have total mass profiles that follow  $\rho_{\text{tot}} \propto r^{-2}$  between a fraction of an effective radius and a few effective radii. Solving the Jeans Equation for a Hernquist luminosity-density profile embedded in a logarithmic potential, we can compute the velocity dispersion profile, depending only on the effective radius ( $R_e$ ), the “Einstein velocity dispersion”

( $\sigma_{\text{Einst}} \equiv \sqrt{GM_E/R_{\text{Einst}}}$ ), and the anisotropy radius ( $r_i$ )

In Fig. 4, we show the luminosity-weighted velocity dispersion profile (in units of  $R_e$  and  $\sigma_{\text{Einst}}$ ), for several values of  $r_i$ . Note that the profiles approach the same curve for large  $R/R_e$  independently of  $r_i$ . Hence, the effect of changing  $r_i$  on the luminosity-weighted velocity dispersion beyond the effective radius, is not as dramatic as in the inner portions of E/S0 galaxies. For this very reason, the luminosity-weighted velocity dispersion does not firmly constrain  $r_i$ . On the other hand, the velocity dispersion profile itself is much more sensitive to  $r_i$ . Therefore, a spatially resolved measurement of  $\sigma(r)$ , extending from a fraction of to a few  $R_e$ , will allow us to constrain both  $r_i$  and the total mass distribution.

To our knowledge, the only system (besides MG2016+112) satisfying the LSD requirements<sup>7</sup> (Sec 1.1), for which velocity dispersion of the lens galaxy has been measured is 0047-281 (Warren et al. 1996, 1998; the effective radius and image separation are measured by Kochanek et al. 2000). As shown in Figure 4, the observed velocity dispersion of the lens galaxy in 0047-281 agrees very well with the value computed with our model. In future papers we will present velocity dispersion (profiles) for other systems, and further test this model.

## 6. SUMMARY & DISCUSSION

### 6.1. Summary

We have shown that the combination of constraints from stellar kinematics and gravitational lensing is extremely powerful in determining the mass profiles of luminous and dark matter in E/S0 galaxies even at very large distances. In particular, for galaxy D in MG2016+112 ( $z = 1.004$ ) we have demonstrated that:

(i) Dark matter is unambiguously present and accounts for >50% (99% CL) of the mass within the Einstein radius. A mass distribution following light with constant  $M/L$  can be ruled out at more than 8- $\sigma$  level. Considering an additional constraint on  $M_*/L_B$  from the evolution of the FP, the smallest allowable fraction of dark matter increases to 60% (99% CL).

(ii) The total mass distribution (dark+luminous) is well described by an isothermal sphere, i.e.  $\rho_{\text{tot}} \propto r^{-\gamma'}$  with  $\gamma' = 2.0 \pm 0.1$ . This result is robust and does not depend significantly on the dynamical state of the system or on the modeling of the mass distribution (one or two component models). The result is only weakly dependent on errors on  $M_E$ ,  $r_i$ ,  $R_e$  and the aperture radius, which in quadrature add at most another 0.1 to the error.

(iii) Using two-component (dark and luminous) spherical models, we find that the inner slope of the dark matter halo  $\gamma < 2.0$  at the 95% CL, i. e. the halo is not isothermal.

(iv) Using a simple adiabatic contraction model, we relate the observed inner slope  $\gamma$  to the inner slope  $\gamma_i$  of the dark matter halo before collapse. In particular we find the upper limit  $\gamma_i < 1.4(2.0)$  at 68(99)% CL, marginally consistent with the high resolution CDM simulations that indicate  $\gamma_i \approx 1.5$  (Ghigna et al. 2000; but see Power et al. 2002 for a discussion of the related uncertainties).

These results are robust because the stellar velocity dis-

persion and gravitational lensing provide two independent mass measurements at two well-separated radii, the effective radius (2.7 kpc) and the Einstein radius (13.7 kpc  $\sim 5R_e$ ). This leads to a very well-defined slope inside the Einstein radius, and to stringent limits on the fraction of dark matter.

Higher signal to noise – and possibly spatially resolved observations – are needed to improve these constraints. However, this is unlikely to be feasible with the current generation of space or ground-based telescopes and will probably need the Next Generation Space Telescope or large ground-based telescopes with adaptive optics. Nevertheless, when the measurement and analysis of the dozen systems targeted by the LSD Survey will be completed, we expect to be able to obtain more stringent constraints by combining the results from the individual systems.

In Sec. 5 we provide a simple test of whether an isothermal total mass distribution is a good description of other lens galaxies. In particular, we compute the luminosity-weighted velocity dispersion profile for a luminous Hernquist component in a logarithmic potential, which depends very mildly on the anisotropy radius, especially at radii larger than  $R_e$ . The measured velocity dispersion of the only system available besides MG2016+112 (0047+281) agrees very well with the curve computed with this model. As new velocity dispersion measurements of E/S0 lens galaxies become available, they can be readily compared to the expectations of this simple model to test whether indeed the isothermal mass profile is a general feature of the E/S0 population.

### 6.2. Discussion

In this paper and KT02 we presented the following simple picture of the lens galaxy D in MG2016+112. The stellar populations are old and metal rich. A significant amount of dark matter is present and the mass distribution of the luminous and dark component are well constrained, reproducing all the available observations.

However, the good agreement of the total mass profile with an  $r^{-2}$  power law calls for a physical explanation. This seems not to be a mere coincidence, given that a similar behavior has been observed in some local ellipticals with kinematic tracers at extraordinary large radii (e. g. Mould et al. 1990; Franx et al. 1994; Rix et al. 1997). Whether this galaxy formed by monolithic collapse, or by mergers of smaller subunits in a hierarchical picture, why do these processes conspire to produce an apparent isothermal mass distribution within  $R_{\text{Einst}}$ ? In the case of adiabatic contraction, there appears to be no reason why gas could not continue to contract or stop earlier and give rise to a total mass distribution that is either steeper or shallower than isothermal. Thus, formation by adiabatic contraction seems not to be a satisfactory explanation, and it is worth seeking a more fundamental explanation. By contrast, complete violent relaxation produces isothermal distribution functions (Lynden-Bell 1967; Shu 1978), and would explain quite naturally the observations. However, this only applies exactly for an infinite mass distribution. When finite mass distributions are considered, (incomplete) violent relaxation leads to an  $R^{1/4}$  luminosity profile (e.g. van Albada 1982; Hjorth & Madsen 1991,

<sup>7</sup> Plus showing no evidence for rotation, since this dynamical model is inappropriate for rotating systems.

1995), which goes as  $r^{-2}$  within the half mass radius, the region of interest here. For the two-component case (luminous and dark), the process should be such as the two components interact to produce the total  $r^{-2}$  density profile, while preserving the segregation of the luminous component in a centrally concentrated density profile (see e.g. the two-component models of Bertin, Saglia & Stiavelli 1992; a similar outcome can be produced by merging of galaxies with massive halos, see e. g. Barnes 1992; Barnes & Hernquist 1996). In the CDM scenario, it is not clear whether the chaotic changes in the gravitational potential during the collapse of halos satisfy the conditions for violent relaxation (e.g. Flores & Primack 1994 and references therein), although it might not be inconceivable that violent relaxation of the inner parts of E/S0 galaxies is close to complete. A complete discussion of these issues goes beyond the aims of this paper. However, we would like to emphasize that whatever physical processes are involved, the mass distribution of galaxy D in MG2016+112 seems already relaxed  $\sim 8$  Gyr ago.

Finally, we note that our poor knowledge of the slope of the mass profile of lens galaxies is the major systematic uncertainty in the determination of  $H_0$  from time-delays (e.g.

Koopmans & Fassnacht 1999; Romanowsky & Kochanek 1999; Koopmans 2001). The assumption of isothermal mass distribution leads to  $H_0 \sim 60-70 \text{ km s}^{-1} \text{ Mpc}^{-1}$  (e.g. Koopmans & Fassnacht 1999; Koopmans 2001), in good agreement with other independent measurements. The result for MG2016+112 seems to indicate that the systematic error – the deviation from isothermality – might indeed be very small for E/S0 lens galaxies. However, the LSD Survey, by measuring the average effective slope of the mass profile and its scatter, will allow us to pin down the largest systematic uncertainty in the global determination of  $H_0$  from gravitational-lens time delays.

We are grateful to E. Agol, A. Benson, G. Bertin, R. Blandford, L. Ciotti, R. Ellis, M. Stiavelli for the stimulating conversations and insightful comments that helped in shaping this manuscript. We acknowledge financial support from NSF and HST grants. Finally, the authors wish to recognize and acknowledge the very significant cultural role and reverence that the summit of Mauna Kea has always had within the indigenous Hawaiian community. We are most fortunate to have the opportunity to conduct observations from this mountain.

## REFERENCES

- Arnaboldi, M. et al. 1996, *ApJ*, 472, 145  
 Barnes, J. 1992, *ApJ*, 393, 484  
 Barnes, J. & Hernquist, L., 1996, *ApJ*, 471, 115  
 Bertin, G., Saglia, R. P., Stiavelli, M., 1992, 384, 423  
 Bertin, G. et al. 1994, *A&A*, 292, 381  
 Bertin, G., & Stiavelli, M., 1993, *Rep. Prog. Phys.*, 56, 493  
 Binney, J. & Tremaine, S., 1987, *Galactic Dynamics*, Princeton University Press, Princeton  
 Borriello, A., Salucci, P., 2001, *MNRAS*, 232, 285  
 Blumenthal, G. R., Faber, S. M., Flores, R., Primack, J. R.  
 Bullock, J. S., Kolatt T. S., Sigad, Y., Somerville, R. S., Kravtsov, A. V., Klypin, A. A., Primack, J. R., & Dekel, A., 2001, *MNRAS*, 321, 598  
 Carollo, C. M., de Zeeuw, P. T., van der Marel, R. P., Danziger, I. J., Qian, E. E., 1995, *ApJ*, 441, L25  
 Ciotti, L., Lanzoni, B., Renzini, A., 1996, *MNRAS*, 282, 1  
 iotti, L., 1999, *ApJ*, 520, 574  
 de Blok, W. J. G. & Bosma, A., 2002, *A&A*, in press (*astro-ph/0201276*)  
 de Blok, W. J. G., McGaugh, S. S., Bosma, A., & Rubin, V. C., 2001, *ApJ*, 552, L23  
 de Zeeuw, T., & Franx, M., 1991, *ARA&A*, 29, 239  
 Djorgovski S. G., Davis M., 1987, *ApJ*, 313, 59  
 Dressler, A., Lynden-Bell, D., Burstein, D., Davies, R. L., Faber, S. M., Terlevich, R., Wegner G. 1987, *ApJ*, 313, 42  
 Flores, R. A. & Primack, J. R. 1994, *ApJ*, 427, L1  
 Franx, M., van Gorkom J. H., & de Zeeuw, P.T. 1994, *ApJ*, 436, 642  
 Gerhard, O., Kronawitter, A., Saglia, R. P., & Bender, R., 2001, *AJ*, 121, 1936  
 Ghigna, S., Moore, B., Governato, F., Lake, G., Quinn, T., Stadel, J., 2000, *ApJ*, 544, 616  
 Hernquist, L., 1990, *ApJ*, 356, 359  
 Hjorth, J. & Madsen, J. 1991, *MNRAS*, 253, 703  
 Hjorth, J. & Madsen, J. 1995, *ApJ*, 445, 55  
 Hui, X., Ford, H. C., Freeman, K. C., Dopita, M. A., 1995, *ApJ*, 449, 592  
 Jimenez, R., Verde, L., Oh, S. P. 2002, *MNRAS*, submitted (*astro-ph/0201352*)  
 Keeton, C. R. 2001, *ApJ*, 561, 46  
 Kochanek, C. S., 1994, *ApJ*, 436, 56  
 Kochanek, C. S., 1995, *ApJ*, 445, 559  
 Kochanek, C. S. et al. 2000, *ApJ*, 543, 131  
 Koopmans, L. V. E., 2001, *PASA*, 18, 179  
 Koopmans, L. V. E. & Fassnacht, C. D., 1999, *ApJ*, 527, 513  
 Koopmans, L. V. E., Garrett, M. A., Blandford, R. D., Lawrence, C. R., Patnaik, A. R., Porcas, R. W., 2001, *MNRAS*, in press (K02)  
 Koopmans, L. V. E. & Treu, T., 2002, *ApJ*, in press, *astro-ph/0201017* (KT02)  
 Lynden-Bell, D., 1967, *MNRAS*, 136, 101  
 McGaugh, S. S. & de Blok, W. J. G. 1998, *ApJ*, 499, 41  
 Merritt, D. 1985a, *AJ*, 90, 1027  
 Merritt, D. 1985b, *MNRAS*, 214, 25  
 Merritt, D., 1999, *PASP*, 111, 129  
 Moore, B., Governato, F., Quinn, T., Stadel, J. & Lake, G., 1998, *ApJ*, 499, L5  
 Mould, J. R., Oke, J. B., de Zeeuw, P. T., Nemec, J. M., 1990, *AJ*, 99, 1823  
 Navarro, J., Frenk, C. S., & White S. D. M., 1997, *ApJ*, 490, 493  
 Osipkov L. P., 1979, *Pis'ma Astron. Zh.*, 5, 77  
 Power, C., Navarro, J. F., Jenkins, A., Frenk C. S., White, S. D. M., Springel, V., Stadel, J., Quinn, T., 2002, *MNRAS*, submitted, *astro-ph/0201544*  
 Romanowsky, A. J. & Kochanek, C. S., 1999, *ApJ*, 516, 18  
 Rix, H. W., de Zeeuw, P. T., Cretton, N., van der Marel, R. P., & Carollo, C. M. 1997, *ApJ*, 488, 702  
 Salucci, P., Burkert, A., 2000, *ApJ*, 537, L9  
 Schade D. et al., 1999, *ApJ*, 525, 31  
 Schneider, P., Ehlers, J. & Falco, E. E. 1992, *Gravitational Lenses*, Springer-Verlag, Berlin.  
 Shu, F. H. 1978, *ApJ*, 225, 83  
 Swaters, R. A., Madore, B. F., & Trewheella, M. 2000, *ApJ*, 531, L107  
 Treu, T., Stiavelli, M., Bertin G., Casertano, C., & Møller, P. 2001, *MNRAS*, 326, 237  
 Treu, T., Stiavelli, M., Casertano, C., Møller, P., & Bertin G. 1999, *MNRAS*, 308, 1307  
 Treu, T., Stiavelli, M., Casertano, C., Møller, P., & Bertin, G. 2002, *ApJ*, 564, L13  
 van Albada, T.S., 1982, *MNRAS*, 201, 939  
 van den Bosch, F. C., Robertson, B. E., Dalcanton, J. J., & de Blok, W. J. G. 2000, *AJ*, 119, 1579  
 van den Bosch, F. C. & Swaters, R. A. 2001, *MNRAS*, 325, 1017  
 van Dokkum, P. G., Franx, M., Kelson D. D. & Illingworth G. D., 1998, *ApJ*, 504, L17  
 Warren, S. J., Hewett, P. C., Lewis, G. F., Møller, P., Iovino, A., Shaver P. A., 1996, *MNRAS*, 278, 139  
 Warren, S. J., Iovino, A., Hewett, P. C., Shaver P. A., 1998, *MNRAS*, 299, 1215